

Production of HHH and HHV ($V = \gamma, Z$) at the hadron colliders

Pankaj Agrawal^{a,b*}, Debashis Saha^{a,b†}, and Ambresh Shivaaji^{c‡}

a) Institute of Physics, Sainik School Post, Bhubaneswar 751 005, India

b) Homi Bhabha National Institute, Training School Complex,

Anushakti Nagar, Mumbai 400085, India

c) Centre for Cosmology, Particle Physics and Phenomenology (CP3)

Universit Catholique de Louvain, B-1348 Louvain-la-Neuve, Belgium

October 1, 2018

Abstract: We consider the production of two Higgs bosons in association with a gauge boson or another Higgs boson at the hadron colliders. We compute the cross sections and distributions for the processes $pp \rightarrow HHH$ and HHZ within the standard model. In particular, we compute the gluon-gluon fusion one-loop contributions mediated via heavy quarks in the loop. It is the leading order contribution to $pp \rightarrow HHH$ process. To the process $pp \rightarrow HHZ$, it is next-to-next-to-leading-order (NNLO) contribution in QCD coupling. We also compare this contribution to the next-to-leading-order (NLO) QCD contribution to this process. The NNLO contribution can be similar to NLO contribution at the Large Hadron Collider (LHC), and significantly more at higher center-of-mass energy machines. We also study new physics effects in these processes by considering ttH , HHH , $HHHH$, HZZ , and $HHZZ$ interactions as anomalous. The anomalous couplings can enhance the cross sections significantly. The $gg \rightarrow HHH$ process is specially sensitive to anomalous trilinear Higgs boson self-coupling. For the $gg \rightarrow HHZ$ process, there is some modest dependence on anomalous HZZ couplings.

Keywords: Electroweak, Higgs boson, LHC, Anomalous couplings

1 Introduction

The CMS and ATLAS Collaborations have been collecting data at the Large Hadron Collider (LHC) for several years [1, 2]. Their major discovery has been of much-anticipated Higgs boson in 2012 [3, 4]. There are many reasons to go beyond the standard model (SM). Since 2012, the search has been going on for any hint for physics beyond the standard model. There have been a number of anomalies that were suspected at different times [5–7], however none has stood test of times. There is no evidence of any signal for beyond the standard model scenarios. A number of popular scenarios involving supersymmetry and large extra dimensions are getting severely constrained [8–11]. Various processes are being analyzed for any hint of a new scenario [1, 2]. In such a situation, exploration of rare

*email: agrawal@iopb.res.in

†email: debasaha@iopb.res.in

‡email: ambresh.shivaaji@uclouvain.be

processes and radiative corrections provide promising avenues to explore. We should note that some other experiments, e. g. LHCb, have reported some unexplained phenomena [12].

At a hadron collider, as centre-of-mass energy increases, so does gluon-gluon luminosity. Therefore, at the LHC and at future probable hadron colliders, the gluons initiated processes would play important role. In this paper, we are considering few such processes. The processes that we consider occur at one-loop level. The gluon-gluon initiated $2 \rightarrow 3$ one-loop processes have been considered in the literature. First full calculation of $gg \rightarrow \gamma\gamma g$ was presented in [13]. Many other authors have also computed the contribution of the gluon-gluon initiated processes on ‘multi-bosons +jets’ [14–26]. These processes are important ingredients for the NLO QCD predictions for $gg \rightarrow BB(B = \gamma, Z, W, H)$ processes [27–31]. These different calculations use different reduction techniques, different packages for computing scalar integrals, and overall different philosophy for the computation. We use our own tensor-reduction code, and have developed a comprehensive package for such calculations.

In this paper, we consider the processes $gg \rightarrow HHH, HH\gamma$, and HHZ , and their contribution to hadron level processes – $pp \rightarrow HHH, HH\gamma$, and HHZ . We presented some preliminary results on these processes along with other Higgs processes in $2 \rightarrow 3$ category in a conference proceeding [32]. Triple Higgs production via gluon fusion has been studied by many authors [33–38]. Plehn and Rauch [33] considered the possibility of measuring quartic Higgs boson coupling in the HHH production. In the reference [35], authors have considered the QCD correction to the HH and HHH production in a Higgs effective field theory approach. The authors in [36–38], have considered the possibility of observing the HHH production at a 100 TeV collider including new physics effects. In Ref. [25] standard model cross sections for a number of loop-induced gluon fusion processes including $gg \rightarrow HHH, HHZ$ are reported. While our work on $pp \rightarrow HHH$ has some overlap with these papers as discussed below, our detailed study of $pp \rightarrow HHZ$ process in SM and beyond is new and being presented here for the first time in the literature. We have also computed using different tools and looked at different aspects of the processes.

The exploration of the production of HHH is important, as it is one of the very few processes where quartic Higgs boson coupling is involved. This process may allow the *direct* measurement of this coupling. With the measurement of self-couplings of the Higgs boson, one can confirm the form of the Higgs potential. Unlike the HHH production, the process $pp \rightarrow HHZ$ gets contribution from the tree-level processes. One can also compute next-to-leading order (NLO) QCD corrections to this tree-level process [39]. In this paper, our focus is on gluon-gluon annihilation contribution, but we also compare it with the LO and NLO contributions. The $gg \rightarrow HHZ$ contribution can be thought of as next-to-next-to-leading order (NNLO) corrections [40]. The production of HHZ is important, as it involves HHH and $HHZZ$ couplings. It is also a background to triple Higgs production process.

In search for new physics scenarios, the use of anomalous interactions may play an important role. This is a model-independent approach which can systematize the search. They may point towards a model that would be suitable to go beyond the standard model. In this paper, we consider possible modification of standard model interactions, inspired by dimension-six operators in effective field theory approach. In particular, we consider the modifications of $ttH, HHH, HHHH, HZZ$, and $HHZZ$ interactions. We study the effects of these anomalous interactions on the production cross sections and on kinematic distributions in $gg \rightarrow HHH, HHZ$ processes. Note that in Refs. [36, 37], the HHH process is studied considering only SM-like deviations in trilinear and quartic couplings. We have in addition considered derivative couplings which have different effects on some distributions as we demonstrate. In Ref. [38], all the CP-even dimension-six operators relevant to HHH process has been considered. In present work, our approach towards new physical effects in HHH process is more phenomenological and we have considered modifications to only those couplings which are present in the standard model at tree-level. For example, we do not consider $ttHH, ttHHH, ggH$ and $ggHH$ interactions. However, for ttH coupling we have considered both CP-even and CP-odd anomalous interactions. Similar approach is taken to study new physics effects in HHZ process.

The paper is organized as follows. In the next section 2, we discuss these various processes and

gluon-gluon annihilation contributions to them. In the section 3, the anomalous contribution to various relevant vertices is discussed. In the section 4, we provide details on the method of calculation and numerous checks. Our numerical results for SM and BSM are presented in section 5. In the last section 6, we present our conclusions.

2 Processes

We consider the gluon-gluon annihilation contribution to the following processes:

$$p p \rightarrow H H \gamma, \quad (1)$$

$$p p \rightarrow H H H, \quad (2)$$

$$p p \rightarrow H H Z. \quad (3)$$

Let us first consider the process $p p \rightarrow H H \gamma$. In the standard model, at tree-level, this process has vanishingly small cross section due to very small light-quark and Higgs boson coupling. At one-loop, there is no contribution to this process from gluon-gluon fusion channel. Using Furry's theorem, one can see that all diagrams contributing to this process add up to zero.

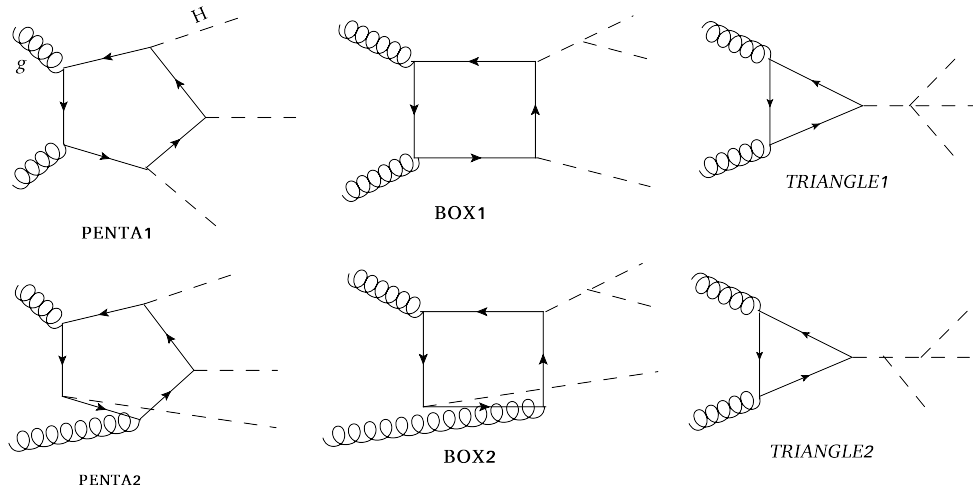


Figure 1: Different classes of diagrams contributing to $gg \rightarrow HHH$ process.

The $p p \rightarrow H H H$ process occurs primarily via $g g \rightarrow H H H$ and leading contribution comes from one-loop diagrams. Because of the very small light-quark and Higgs boson couplings, the tree level process $q \bar{q} \rightarrow H H H$ makes very small contribution. Therefore, we only consider the contribution of the $g g \rightarrow H H H$ process. This is a one-loop process. There are 24 pentagon, 18 box, and 8 triangle diagrams contributing to the process for each quark flavor in the loop. There are some more diagrams in the box and triangle categories at one-loop level, but their contributions are zero, as they do not conserve color charge ($\text{Tr}(\lambda^a)=0$). In the loop, a light-quark would not contribute due to very small Yukawa coupling; so we keep only diagrams with a top-quark and a bottom quark. We do not need to numerically compute all the diagrams separately, as many diagrams are related to one another by charge conjugation symmetry, or crossing. We can compute all the diagrams using six prototype diagrams as shown in Fig. 1. By permuting the legs in the prototype diagrams, and using charge conjugation (Furry's theorem), all the amplitudes can be calculated. Out of 24 ($=4!$) pentagon diagrams, we had to numerically calculate only 12 diagrams as other 12 diagrams can be related to the previous diagrams by Furry's theorem. Out of these 12 pentagon diagrams, 6 ($=3!$) diagrams can be obtained from PENTA1 prototype diagram by permuting the Higgs bosons; other 6 diagrams can be obtained similarly from

PENTA2 prototype diagram. Similarly, out of 18 box diagrams, we need to numerically compute only 9 diagrams, and from these the rest can be found out using Furry's theorem only. Out of these 9 box diagrams, 6 can be calculated from BOX1 prototype diagram by permuting Higgs bosons in six different ways. Other 3 box diagrams can be obtained by the permutation of external Higgs boson in BOX2 prototype diagram. Out of 8 triangle diagrams, we need to numerically compute only 4; TRIANGLE1 prototype diagram gives one of these and TRIANGLE2 prototype diagram gives the rest 3 diagrams by permuting external Higgs bosons.

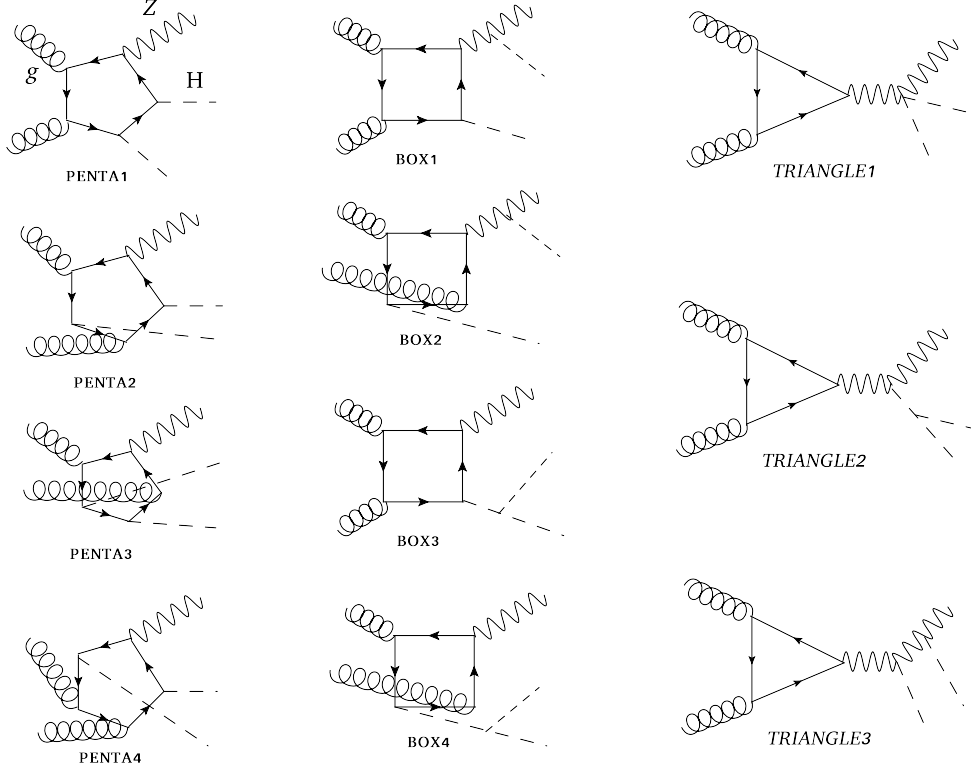


Figure 2: Different classes of diagrams contributing to $gg \rightarrow HHZ$ process.

The $pp \rightarrow HHZ$ can occur at tree level through quark-antiquark annihilation. The cross section is large enough for it to be observable with high luminosity option. One can also compute NLO QCD corrections to this process easily. Our focus will be contribution of gluon-gluon fusion process: $gg \rightarrow HHZ$ which occurs at the one-loop level. Formally this contribution is of NNLO order. However, as we shall see, at the LHC, this contribution can be of the same order as the NLO corrections. Due to enhanced gluon-gluon luminosity at larger center-of-mass energies, this NNLO correction will even dominate over NLO correction at higher energy hadron colliders. There are 24 pentagon, 18 box, and 8 triangle diagrams contributing to the process $gg \rightarrow HHZ$. Like in the case $gg \rightarrow HHH$, here also the diagrams are divided into many prototype classes as shown in Fig. 2. Here, as before, out of 24 pentagon, 18 box, and 8 triangle diagrams, we need to numerically compute only 12 pentagon, 9 box, and 4 triangle diagrams respectively. Out of these 12 pentagon diagrams, each of PENTA1 and PENTA2 prototype diagrams gives four diagrams, and each of PENTA3 and PENTA4 prototype diagrams gives two diagrams. In the case of box diagrams, BOX1, BOX2, BOX3, and BOX4 prototype diagrams give 4, 2, 2, and 1 diagrams respectively. There are three prototype triangle diagrams – TRIANGLE1, TRIANGLE2, and TRIANGLE3; these prototype diagrams give 1, 1, and 2 diagrams respectively. Note that due to Furry's theorem only the axial-vector part of the Z boson coupling with the quarks in the loop contributes. Feynman diagrams in Fig. 1 and Fig. 2 have been made using

JaxoDraw [41]. Computation of one-loop diagrams in $gg \rightarrow HHH, HHZ$ processes are described in section 4.

3 Anomalous interactions of Higgs boson

There are a number of arguments for going beyond the standard model. In absence of any new resonance at the LHC, one way to consider the effects of beyond-the-standard-model scenarios is to consider the possible modification of standard model vertices. We are mainly interested in anomalous couplings of the Higgs boson which would affect the processes under consideration. These include, $ttH, HZZ, HHZZ, HHH$ and $HHHH$ interactions. Some of them, for example, ttH and HZZ are already constrained by the existing LHC data [42]. The trilinear Higgs self coupling is very weakly constrained by the data [43] and couplings $HHZZ$ and $HHHH$ are unconstrained at present. In the following, we consider most general interaction Lagrangian incorporating the BSM physics which would lead to deviations in the Higgs couplings of our interests.

3.1 Anomalous $\bar{t}tH$ Vertex

In the standard model, the top quark couples with the Higgs boson via the Yukawa coupling. This leads to a scalar ttH coupling. The most general vertex for $\bar{t}tH$ interaction can be parametrized as,

$$\mathcal{L}_{\bar{t}tH} = -\frac{m_t}{v}\bar{t}[(1 + \kappa_t) + i\tilde{\kappa}_t\gamma_5]tH. \quad (4)$$

Here v is electroweak symmetry breaking scale and it is approximately 247 GeV. In the standard model, $\kappa_t = \tilde{\kappa}_t = 0$. We use following bounds for κ_t and $\tilde{\kappa}_t$ [44, 45]:

$$\begin{aligned} -0.2 &\leq \kappa_t \leq 0.2, \\ -0.1 &\leq \tilde{\kappa}_t \leq 0.1. \end{aligned} \quad (5)$$

This vertex contributes to both HHH and HHZ production. As we shall see, the scaling of the scalar coupling, as parametrized by κ_t can change the cross section significantly.

3.2 Anomalous HHH and $HHHH$ Vertices

After the discovery of the Higgs boson, one of the important task is to determine the form of the Higgs potential. As discussed before, one of the characteristic feature of the Higgs potential in the standard model is specific form of Higgs boson self-couplings. The Higgs boson self-interactions can be expressed in terms of the anomalous couplings as

$$\mathcal{L}_{HHH} = -\frac{3m_H^2}{v} \left(\frac{1}{6}(1 + g_{3H}^{(0)}) H^3 + \frac{1}{6m_H^2} g_{3H}^{(1)} H \partial_\mu H \partial^\mu H \right), \quad (6)$$

$$\mathcal{L}_{HHHH} = -\frac{3m_H^2}{v^2} \left(\frac{1}{24}(1 + g_{4H}^{(0)}) H^4 + \frac{1}{24m_H^2} g_{4H}^{(1)} H^2 \partial_\mu H \partial^\mu H \right). \quad (7)$$

In the SM, $g_{3H}^{(0)} = g_{4H}^{(0)} = g_{3H}^{(1)} = g_{4H}^{(1)} = 0$. Here $g_{3H}^{(0)}$ and $g_{4H}^{(0)}$ just scale the trilinear and quartic Higgs boson self-couplings, respectively. Both of these couplings occur in HHH production. In the HHZ production, only trilinear coupling occurs. As we shall see, both the processes are sensitive to modification of trilinear coupling. These couplings are poorly determined, as they occur in processes with small cross section. It may take a decade or more before a serious bound can be put on these couplings. For illustration, we take these parameters in the range between -1.0 to 1.0.

3.3 Anomalous HZZ and $HHZZ$ vertices

These two vertices occur in the process $gg \rightarrow HHZ$. While HZZ vertex occurs in other processes, like $pp \rightarrow HZ$, the vertex $HHZZ$ occurs mainly in processes involving double Higgs boson production, so is poorly constrained. The most general HZZ interaction that can be written has following form,

$$\mathcal{L}_{HZZ} = \frac{gM_Z}{c_W} \left\{ \frac{1}{2}(1 + g_{HZZ}^{(0)})HZ_\mu Z^\mu - \frac{1}{4M_Z^2}g_{HZZ}^{(1)}HZ_{\mu\nu}Z^{\mu\nu} - \frac{1}{M_Z^2}g_{HZZ}^{(2)}HZ_\nu\partial_\mu Z^{\mu\nu} \right\}. \quad (8)$$

In the above g is the coupling parameter of the $SU(2)_L$ group and $c_W = \cos\theta_W$, θ_W being the weak angle. The SM HZZ interaction corresponds to $g_{HZZ}^{(0)} = g_{HZZ}^{(1)} = g_{HZZ}^{(2)} = 0$. This interaction has derivative couplings which lead to momentum dependence. This is unlike standard model.

The following are the various bounds on the anomalous coupling parameters [46]

$$\begin{aligned} -0.10 &\leq g_{HZZ}^{(0)} \leq 0.10, \\ -0.09 &\leq g_{HZZ}^{(1)} \leq 0.04, \\ -0.07 &\leq g_{HZZ}^{(2)} \leq 0.03. \end{aligned} \quad (9)$$

There is also modification of $HHZZ$ coupling. This modification only scales the standard model interactions:

$$\mathcal{L}_{HHZZ} = \frac{gM_Z}{c_W v} \left\{ \frac{1}{4}(1 + g_{HHZZ}^{(0)})HHZ_\mu Z^\mu \right\}. \quad (10)$$

In the SM, $g_{HHZZ}^{(0)} = 0$. In absence of any available bound for this coupling, we allow the parameter $g_{HHZZ}^{(0)}$ to vary between -0.1 and 0.1.

The anomalous interactions mentioned above are well motivated within the framework of an effective field theory in which the new physics effects are parametrized in terms of higher dimensional operators. These operators are constructed from the SM fields and respect the symmetries of the SM. A complete list of independent dimension-six operators is now available [47–49]. The anomalous couplings introduced above are related to the Wilson coefficients of these operators [50–54].

The Feynman rules for the anomalous Higgs vertices are listed in the appendix A. As we shall see, in the allowed range of the parameter values, the contribution of the anomalous vertices can be important in our processes. Note that even in the presence of these anomalous couplings the amplitude for $gg \rightarrow HH\gamma$ process does not receive any contribution.

4 Calculation and Checks

As discussed in the section 2, we compute prototype pentagon, box, and triangle diagrams. Then by using crossing and Furry's theorem, we can compute rest of the diagrams. All the diagrams have a fermion loop, so to calculate the amplitude we need to compute trace of a string of gamma matrices. We calculate the traces of the prototypes diagrams using FORM [55]. The process $gg \rightarrow HHZ$ includes ttZ coupling, which has both vector and axial vector parts. The presence of γ_5 requires special care, due to the potential presence of anomalies. We have handled this situation in two different ways. Since the process is free from UV divergences, we can take trace in four dimensions. We have also calculated the trace in n dimensions using Larin's prescription for γ_5 [56,57]. Both methods, in the end give same results when the contributions from both the top and bottom quark loops are considered. When we include ttH anomalous pseudo-scalar coupling, the trace will include more γ_5 matrices for both HHH and HHZ production.

In the first step, we use `FORM` to take the trace and write the amplitude in terms of tensor and scalar integrals. We use an in-house package `OVRReduce` to reduce tensor integrals to lower-point tensor integrals and scalar integrals in dimensional regularization. This package is based on the methods of Oldenborgh and Vermaseren [21, 58]. After the reduction, all that we need to do is to compute various scalar integrals of box, triangle, and bubble types. To compute these scalar integrals, we use `OneL0op` library by Andreas van Hameren [59]. It uses dimensional regularization to regulate UV and IR divergences. For the pentagon scalar integrals, we use van Neerven-Vermaseren technique [21, 60]. As the amplitudes are quite large and complicated, we first compute helicity amplitude for a process numerically before squaring it. The Monte Carlo integration over the entire phase space has been performed using `VEGAS` code [61] as implemented in `AMCI` (Advanced Monte Carlo Integration) package [62]. `AMCI` implements a parallel version of `VEGAS` algorithm which makes use of Parallel Virtual Machine (PVM) software [63].

While performing multi-leg one loop calculations, the issue of numerical instability comes in for certain phase space points. As the number of such points are not large, and contribution of these phase space points is not expected to be large, as is the practice, we exclude these phase space points by setting a suitable upper bound on the amplitude-squared¹. This upper bound is chosen after finding out possible values the amplitude-squared can have by running the code. This upper bound is increased until we hit the unstable phase space point. The cross section remains stable and does not change, even when this upper bound is increased by several orders of magnitude. For the HHH process, we do not come across any unstable phase space point. For the $gg \rightarrow HHZ$ process, the number of unstable points are well below 0.002%.

We have performed many checks to verify the correctness of the amplitude for each process. These checks include verification of cancellation of UV & IR divergences and gauge invariance. Because of the presence of the Higgs boson in the final state, we have only top and bottom quarks in the loop. In both the processes, all pentagon, box, and triangle diagrams are therefore separately IR finite. Overall amplitude at any phase space point is UV finite. Each pentagon diagram is UV finite, which is again as expected as simple power counting reveals it. Individual box diagrams are also UV finite, since one will have at most two (three)-tensor box integrals in $gg \rightarrow HHH(HHZ)$. Each triangle diagram is also UV finite. In both these processes, we have verified that in the large top quark mass limit the amplitude becomes constant implying non-decoupling of top quark in $m_t \rightarrow \infty$ limit [64].

To check gauge invariance, we replace the polarization vector of a gluon with its momenta in the amplitude. In $gg \rightarrow HHH$, the overall amplitude has been checked to be gauge invariant with respect to both the gluons. We find that each triangle diagram is individually gauge invariant, while each pentagon and box diagram is not. However, all pentagon diagrams together, and all box diagrams together are gauge invariant. Here interesting point is that the pentagon, box, and triangle diagrams are separately gauge invariant with respect to the gluons². So it may be tempting to use only one class of diagrams to compute the cross section. However as will see below, it can lead to serious errors. Here we have done the calculation only in four dimension. The amplitude is found to be gauge invariant for both gluons in the presence of pseudo-scalar coupling even when we consider only one quark.

We have calculated the $gg \rightarrow HHZ$ amplitude treating γ_5 in four-dimension and in n -dimension using Larin's prescription [56]. In four-dimension, if we consider only one quark, each triangle diagram is gauge invariant with respect to one gluon but not for the other. All the triangle diagrams taken together are also not gauge invariant for the other gluon. However, if we consider both top and bottom quarks in the amplitude, each triangle diagram is gauge invariant for both gluons. This is related to the quantum anomaly associated with the axial vector coupling of Z boson with fermions. None of the pentagon or box diagram is individually gauge invariant for any gluon. However, referring to Fig. 2, all the pentagon diagrams taken together, or all the diagrams of BOX1 and BOX2 classes together, or all the diagrams of BOX3 and BOX4 classes together are gauge invariant for both gluons. In n -

¹We have cross-checked the robustness of this procedure by comparing it with another implementation of rejecting unstable phase space points based on Ward-identity or gauge invariance check for each phase space point [21].

²With respect to SM EW symmetry only full amplitude is meaningful.

dimension, all the pentagon diagrams together, all the BOX1 and BOX2 diagrams together, all the BOX3 and BOX4 diagrams together, and each triangle diagram are gauge invariant with respect to the both gluons for top and bottom quarks separately. In any case, to remove the anomaly associated with the chiral current of Z boson the contributions from both the top and bottom quarks in the loop must be included.

5 Numerical results

In our computation of cross sections and distributions we have used: $p_T^{H,Z} > 1$ GeV, $|y^{H,Z}| < 5$. The cut on the p_T of the Higgs boson and the Z boson (of 1 GeV) is there to reduce the number of phase space points which introduce numerical instability. We have checked and it can be understood from the p_T distributions presented below that the effect of removing the cut is negligible. The results for gluon fusion processes are obtained using `cteq611` parton distribution functions [65], and using $\mu_R = \mu_F = \sqrt{\hat{s}}$ (partonic center-of-mass energy) as the renormalization and factorization scales. We have also included uncertainties in the results for the LHC by varying the renormalization and factorization scales by a factor of 2. The scale uncertainties are listed in the table³.

5.1 The process $pp \rightarrow HHH$

In Table 1, we present the cross section for this process at the LHC center-of-mass energy, and at other proposed hadronic colliders. The cross section at 13 TeV center-of-mass energy is 32.0 attobarn. So as of now only 2-3 such events may have been produced at the LHC. With even expected 3 ab^{-1} luminosity, there will be only about 100 events. At 100 TeV, thanks to a larger gluon flux, the cross section will be 100 times larger. Note that these cross sections suffer from large scale uncertainty (-22% to 31% at 13 TeV) which is typical to gluon fusion processes. These uncertainties are large due to the significant dependence of the strong coupling constant, $\alpha_s(\mu)$, on the renormalization scale. As center of mass energy increases, the coupling constant value decreases, so does the dependence of the cross section on the renormalization scale.

\sqrt{s} [TeV]	8	13	33	100
$\sigma_{GG}^{HHH,LO}$ [ab]	$7.0^{+34.6\%}_{-24.0\%}$	$32.0^{+30.6\%}_{-22.2\%}$	$330.8^{+23.8\%}_{-18.4\%}$	$3121.1^{+17.4\%}_{-14.1\%}$

Table 1: $pp \rightarrow HHH$ hadronic cross sections and corresponding scale uncertainties in the SM at different collider center-of-mass energies.

In the Table 2, we have displayed the values of cross sections when only pentagon, or box, or triangle type diagrams are considered. These categories of diagrams are separately gauge invariant with respect to the gluons. So if we wish to estimate cross section by only keeping a category of diagrams, we will make an order of magnitude error. This is because there is large destructive interference among these categories of diagrams. If for simplicity, we include only triangle diagrams in the calculation, we will underestimate the cross section, while inclusion of only box or pentagon diagrams will overestimate the cross section. For 13 TeV centre-of-mass energy we see that the total cross section is about 32.0 attobarn, whereas penta, box, and triangle class contribute 94.4, 53.6, and 3.5 attobarn respectively.

³With the CT14, the latest version of CTEQ parton distributions, the cross section for the process $pp \rightarrow HHH$ changes by about 13% at 13 TeV center-of-mass-energy and by about 4% at 100 TeV center-of-mass-energy.

\sqrt{s} [TeV]	8	13	33	100
$\sigma_{\text{penta}}^{\text{HHH}}$ [ab]	22.1	94.4	916.4	8067.8
$\sigma_{\text{box}}^{\text{HHH}}$ [ab]	12.9	53.6	502.5	4287.4
$\sigma_{\text{triangle}}^{\text{HHH}}$ [ab]	0.8	3.5	32.1	270.8
$\sigma_{\text{total}}^{\text{HHH}}$ [ab]	7.0	32.0	330.3	3121.3

Table 2: SM contribution of pentagon, box, and triangle diagrams to the total cross section in $gg \rightarrow HHH$ at different collider center-of-mass energies, displaying a destructive interference effect.

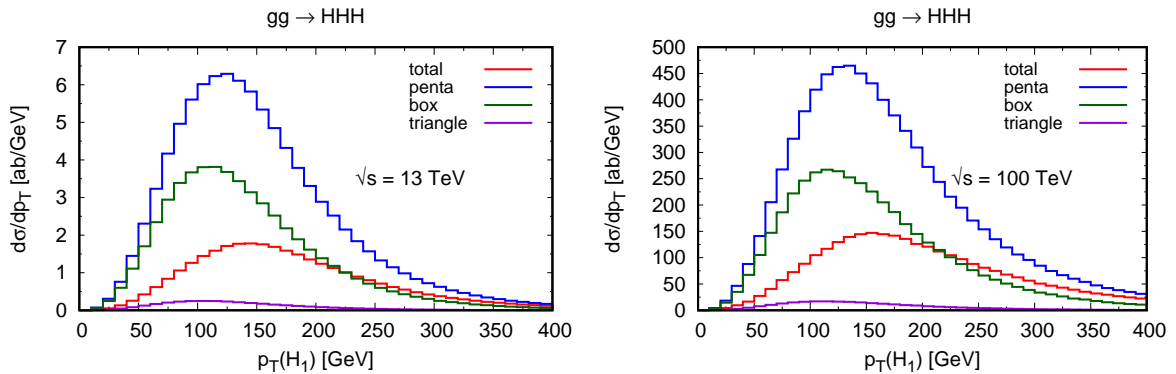


Figure 3: SM contribution of pentagon (blue), box (green), and triangle (violet) diagrams to leading $p_T(H)$ distribution in $gg \rightarrow HHH$ at 13 TeV (left) and 100 TeV (right).

This shows that there is strong destructive interference between the different categories of diagrams. At higher center-of-mass energies the interference effect becomes smaller. If one takes the Higgs effective field theory approach, there would be inclusion of triangle type diagrams only, and the cross section would be underestimated.

In Fig. 3, we have plotted the contribution of various category of diagrams with respect to the p_T of the leading Higgs boson at $\sqrt{s} = 13$ TeV and 100 TeV. We see that it is the pentagon type diagrams, which give harder Higgs boson, than other categories of diagrams. Interference kills such events and the p_T peaks between 130 and 160 GeV. In Fig. 4, we have plotted a number of physical quantities involving leading, next-to-leading, and next-to-next-to-leading Higgs bosons arranged according to their transverse momenta. As would be expected leading Higgs boson's p_T is harder and peaks around 140-160 GeV. Softest Higgs boson p_T is mostly around 50 GeV with a large tail. However all three types are produced mainly centrally. The leading and next-to-leading Higgs bosons are produced more back-to-back than other Higgs bosons. Two of the softer Higgs bosons are produced closer to each other. The masses of the Higgs boson pair also show expected behavior. The mass of the two larger p_T Higgs bosons has a peak about 375 GeV, while for the two softer Higgs boson, it is near the twice of the mass

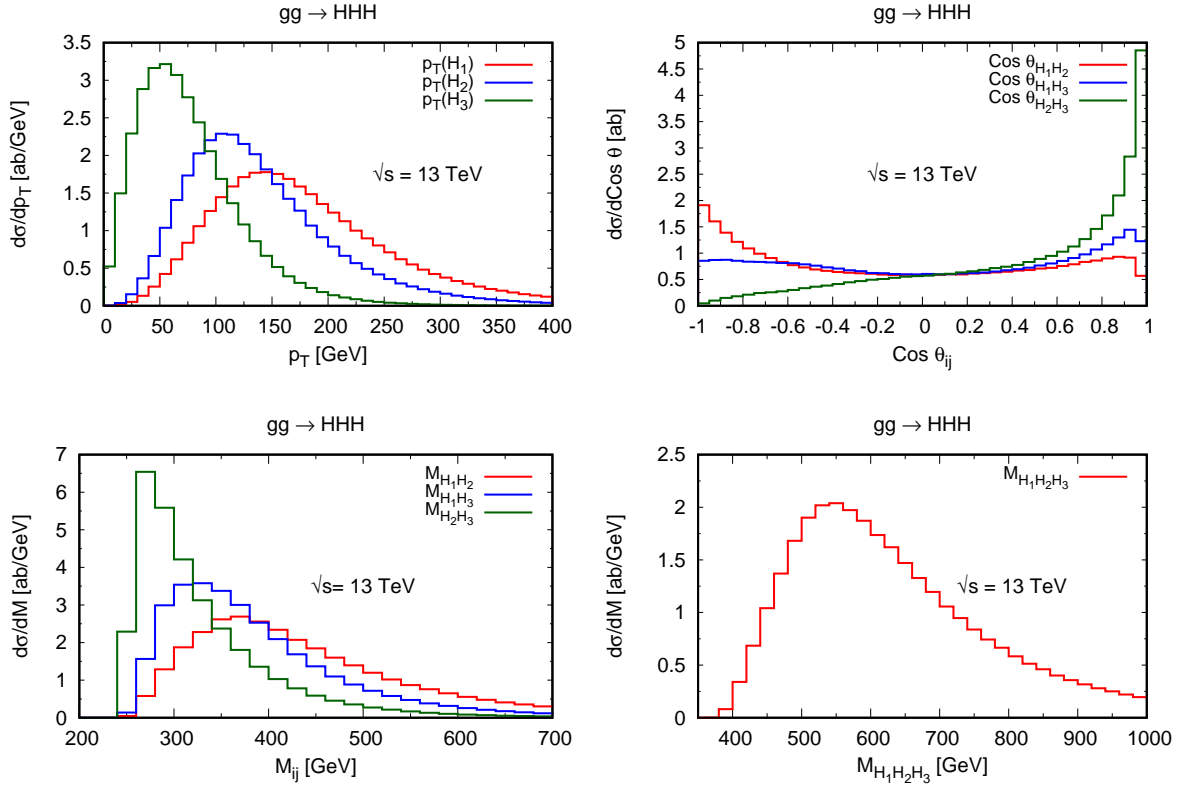


Figure 4: Kinematic distributions for $gg \rightarrow HHH$ in the SM at 13 TeV. These plots are obtained after p_T ordering the Higgs bosons. $H_1, H_2,$ and H_3 refer to the hardest, second hardest, and third hardest Higgs bosons in p_T respectively.

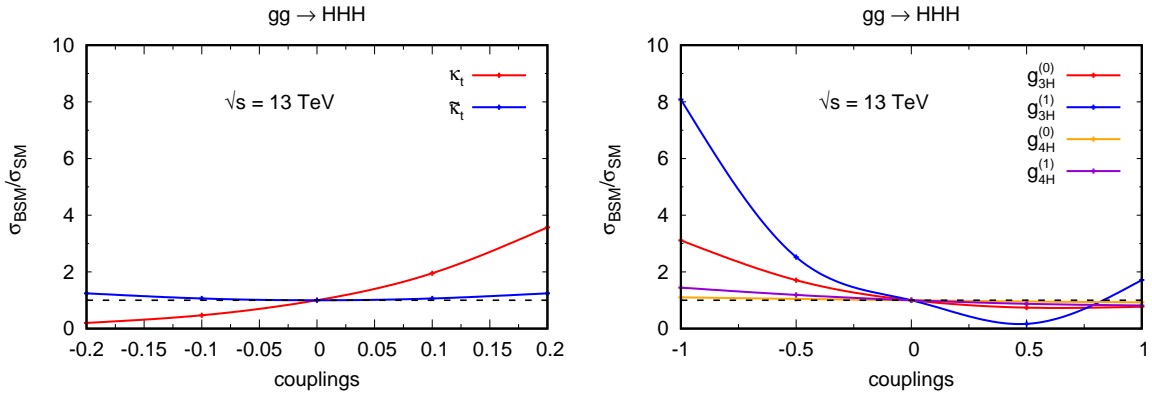


Figure 5: $\frac{\sigma_{\text{BSM}}}{\sigma_{\text{SM}}}$ as function of various Higgs anomalous couplings affecting $gg \rightarrow HHH$ at 13 TeV.

of the Higgs boson. The invariant mass of the three Higgs bosons peak around 550 GeV. At higher center-of-mass energy, 100 TeV, the behavior of physical quantities is largely the same, so we have not given separate plots.

In Fig. 5, we have plotted the ratios of the cross section with various anomalous couplings and the standard model cross section. We have plotted for the range of parameters mentioned in section 3, except for $\tilde{\kappa}_t$ for which we have doubled the range. We see that the cross section is not sensitive to the pseudo-scalar ttH coupling and modification of quartic Higgs boson coupling. It is not surprising

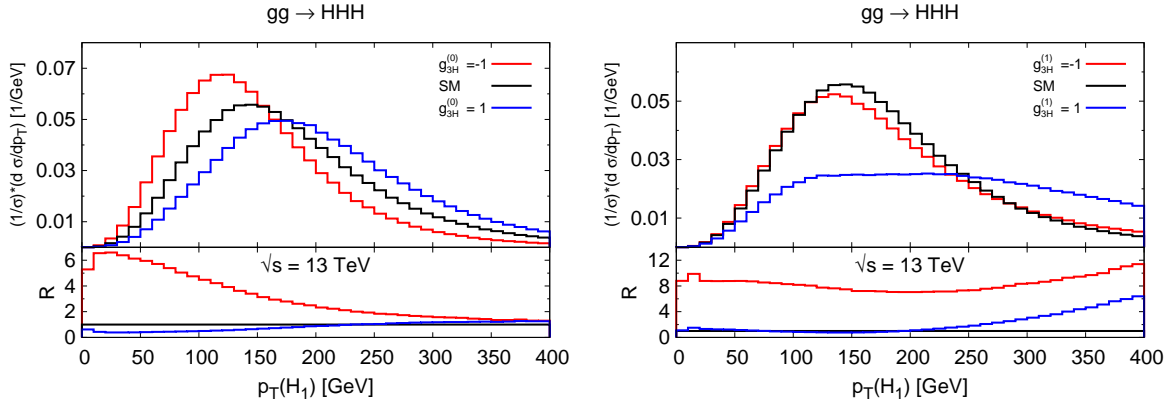


Figure 6: Normalized leading $p_T(H)$ distribution in $gg \rightarrow HHH$ at 13 TeV for some benchmark values of anomalous trilinear Higgs self-coupling. In the lower panels R is defined as the ratio of the distributions $(d\sigma/dp_T)$ in BSM and in SM.

because of three Higgs boson coming out of same vertex, requiring the fourth Higgs boson to be far off-shell. However, it is sensitive to the scaling of the scalar ttH coupling. Cross section can significantly change with the change in this coupling – by a factor of 3-4. The cross section is also sensitive to the sign of this coupling. Interestingly, the cross section is sensitive to trilinear Higgs boson coupling too. Cross section can increase by an order of magnitude by the change of derivative coupling, $g_{3H}^{(1)}$. This coupling is momentum dependent and will have larger effect at higher center-of-mass energy machine. The scaling of the coupling, $g_{3H}^{(0)}$, can also change the cross section by about a factor of 3. If one could detect HHH events at a future collider, one can probe trilinear coupling easily. Looking at Fig. 6, we see that the scaling of the coupling changes the low p_T (of the leading Higgs boson) events more; while derivative coupling tends to also change large p_T events. Therefore, one can probe both couplings by focusing on low p_T events in one case and higher p_T events in another case. The p_T distributions for the sub-leading Higgs boson and mass distributions of two or three Higgs bosons show similar sensitivity. Note that the cross-section is symmetric for $\tilde{\kappa}_t$.

Let us now consider the possibility of observing the production of the three Higgs bosons, HHH . At the LHC, the cross section is of the order of 32 ab. It leads to too few events with even the highest possible integrated luminosity of 3 ab^{-1} to be observable in the sea of the background. However we have seen that this process is sensitive to trilinear Higgs boson self-coupling. Such anomalous couplings can enhance the cross section by a factor of 3 to 8. Even with this enhancement, once we include branching ratios, kinematic cuts, tagging, and other efficiencies, there will be too few events to be visible. Given that it is one of the few processes to help determine the quartic Higgs boson self-coupling, it will be worthwhile to look for this process. At a 100 TeV machine, it could be possible. The cross section there is about 3100 ab. With large enough data, this process might be observable. The process $pp \rightarrow HHH$ will give rise to ‘multileptons’ and ‘few leptons with jets’ signatures. There will be irreducible background from ZZZ production, and an array of reducible backgrounds depending on the signature. The ZZZ production cross section is about 136 fb which can be controlled if we include branching ratios and construct Higgs boson masses. In the case of reducible backgrounds there will be background from a top-pair production with jets or vector bosons, multi vector boson production with jets, and multijets. To tame these backgrounds, one may require tagging of bottom jets and tau jets. Given the severity of the background, one may still need a multivariate analysis. In [36], authors have studied the the channel $HHH \rightarrow b\bar{b}b\bar{b}\gamma\gamma$ in the standard model and its simple deformation with marginal success. More recently the authors of [37] have studied ‘ $b\bar{b}b\bar{b}\tau\tau$ ’ channel and authors in [38] have similarly studied ‘ $b\bar{b}l^+l^- + 4 \text{ jets}$ ’ channel with modest success. Therefore, a modification of the

interactions that will enhance the signal significantly and improved search strategies will be needed to determine Higgs boson self-couplings.

5.2 The process $pp \rightarrow HHZ$

Unlike the $pp \rightarrow HHH$ process, this process can occur at the tree level. In this section, we will mainly focus the NNLO contribution to this process that occur via $gg \rightarrow HHZ$ process. We have estimated tree level value and one-loop QCD corrections, i. e., NLO contribution using `MadGraph5_aMC@NLO` [66]. We will see that NNLO contribution is comparable to NLO contribution at 13 TeV. NNLO contribution becomes even more important as the center-of-mass energy increases, and can become comparable to the tree level value.

\sqrt{s} (TeV)	8	13	33	100
$\sigma_{GG}^{HHZ,LO}$ [ab]	10.0 ^{+34.0%} _{-24.0%}	42.3 ^{+30.9%} _{-21.4%}	406.7 ^{+23.9%} _{-17.9%}	3562.4 ^{+16.8%} _{-13.9%}
$\sigma_{QQ}^{HHZ,LO}$ [ab]	97.2 ^{+3.9%} _{-3.8%}	236.7 ^{+1.3%} _{-1.5%}	988.8 ^{+2.6%} _{-3.3%}	4393.0 ^{+7.1%} _{-7.8%}
$\sigma_{QQ}^{HHZ,NLO}$ [ab]	122.0 ^{+1.7%} _{-1.6%}	294.5 ^{+1.5%} _{-1.0%}	1197.0 ^{+1.7%} _{-1.9%}	4971.0 ^{+1.8%} _{-3.2%}
$R_1 = \frac{\sigma_{GG}^{HHZ,LO}}{\sigma_{QQ}^{HHZ,LO}}$	0.10	0.18	0.41	0.81
$R_2 = \frac{\sigma_{GG}^{HHZ,LO}}{\sigma_{QQ}^{HHZ,NLO}}$	0.08	0.14	0.34	0.72
$R_3 = \frac{\sigma_{GG}^{HHZ,LO}}{(\sigma_{QQ}^{HHZ,NLO} - \sigma_{QQ}^{HHZ,LO})}$	0.40	0.73	1.95	6.16

Table 3: A comparison of different perturbative orders in QCD coupling contributing to $pp \rightarrow HHZ$ hadronic cross section at $\sqrt{s} = 8, 13, 33,$ and 100 TeV. We also calculate ratios R_1 , R_2 and R_3 which quantify the GG contribution with respect to the $QQ(LO)$ and $QQ(NLO)$ contributions.

In Table 3, we have given LO, NLO, and NNLO contribution to this process at different center-of-mass energies. We have used `cteq611` parton distribution for LO and NNLO calculation and `cteq6m` for the NLO calculation [65], with \hat{s} as renormalization/factorization scales for NNLO calculation and sum of transverse mass for LO and NLO calculation (in `MadGraph5_aMC@NLO`). Uncertainties are estimated by using other `cteq6` parton distributions and changing the renormalization/factorization scales by a factor of 2. At the LHC, the leading order contribution is about 237 ab. NLO corrections are about 24%, and add 57.8 ab to the LO value. NNLO corrections are about 18%, and add 42.3 ab to the LO value. The cross section including LO, NLO, and NNLO values is about 336.8 ab, leading to about 1000 events at the maximal proposed integrated luminosity. As in the case of HHH production, the value of NNLO contribution becomes more significant as center-of-mass energy increases. At 100 TeV, NLO correction is only 13%, while NNLO contribution is 81% of the LO value due to an increase in the gluon flux. We see that NNLO contribution approaches the LO value. It is however not alarming, only more useful. NNLO contribution is from gluon-gluon annihilation, while LO result is from quark-antiquark scattering. At 13 TeV, the scale uncertainties for GG channel are in the range of -21% to 31%. The reason for this large uncertainty and its decrease with center of mass energy is same as that for $gg \rightarrow HHH$ process. Uncertainties in the QQ processes are smaller, as these are primarily

electroweak processes.

\sqrt{s} (TeV)	8	13	33	100
$\sigma_{\text{penta}}^{\text{HHZ}}$ [ab]	30.8	148.1	1718.4	17694.0
$\sigma_{\text{box}}^{\text{HHZ}}$ [ab]	73.1	434.7	7468.2	115747.2
$\sigma_{\text{triangle}}^{\text{HHZ}}$ [ab]	78.4	475.6	8157.2	124273.1
$\sigma_{\text{total}}^{\text{HHZ}}$ [ab]	10.0	42.3	406.4	3557.5

Table 4: SM contribution of pentagon, box, and triangle diagrams to the total cross section in $gg \rightarrow HHZ$ at different collider center-of-mass energies, displaying a destructive interference effect.

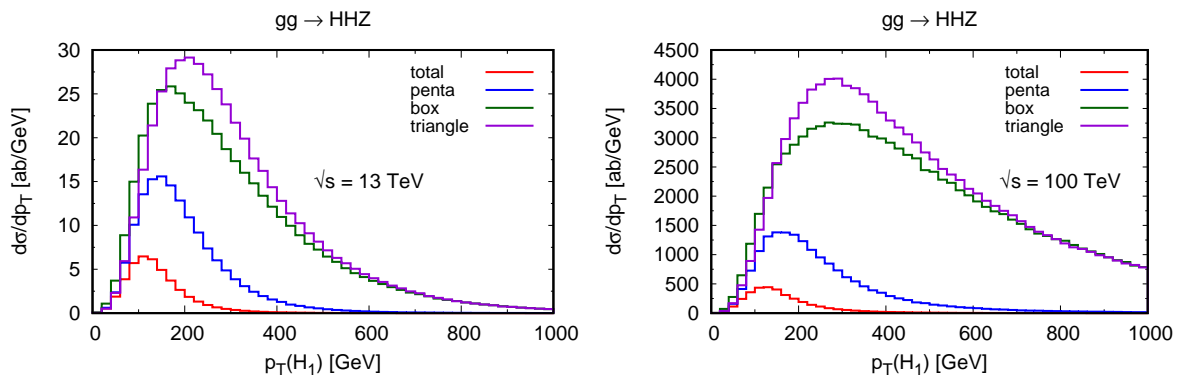


Figure 7: SM contribution of pentagon (blue), box (green) and triangle (violet) diagrams to leading $p_T(H)$ distribution in $gg \rightarrow HHZ$ at 13 TeV (left) and 100 TeV (right).

Table 4 demonstrates interference effect in the process HHZ . Unlike HHH process, here triangle diagram contribution is larger and interference effect is more severe. If we keep only one class of diagrams which are gauge invariant with respect to the gluons, we will overestimate the cross section by an order of magnitude at 13 TeV. We see that the total cross section is 42.3 attobarn, whereas penta, box, and triangle class contribute 148.1, 434.7, and 475.6 attobarn respectively. This shows there is a strong destructive interference between the different class of diagrams. The destructive interference effect becomes stronger at higher \sqrt{s} . In Fig. 7, we have plotted the contribution of the individual class of diagrams with respect to the p_T of the leading (in p_T) Higgs boson. Here effects are different. Triangle and box diagrams have larger cross section and contribute more to higher p_T events. The interference effects seem to cut off large p_T contribution of the individual class of diagrams. The p_T of the leading Higgs boson, after the interference, shifts to lower values and peaks around 120 GeV.

In Fig. 8, we have plotted a few physical quantities, as in the case of HHH production for 13 TeV LHC. The p_T distribution of the leading Higgs bosons and Z boson are similar. Both peaks around 110 GeV. As would be expected, the leading Higgs boson's p_T is harder than next-to-leading Higgs

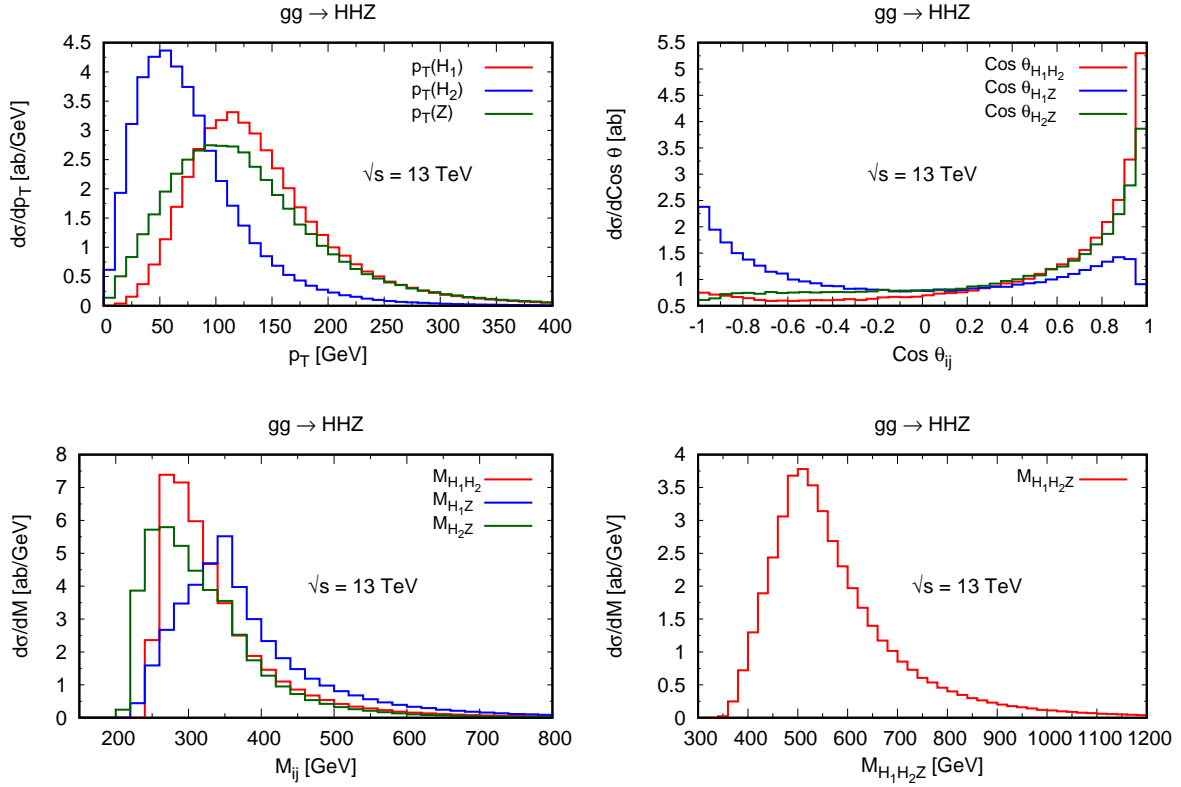


Figure 8: Kinematic distributions for $gg \rightarrow HHZ$ in the SM at 13 TeV. These plots are obtained after p_T ordering the Higgs bosons. H_1 and H_2 refer to the hardest and second hardest Higgs bosons in p_T respectively.

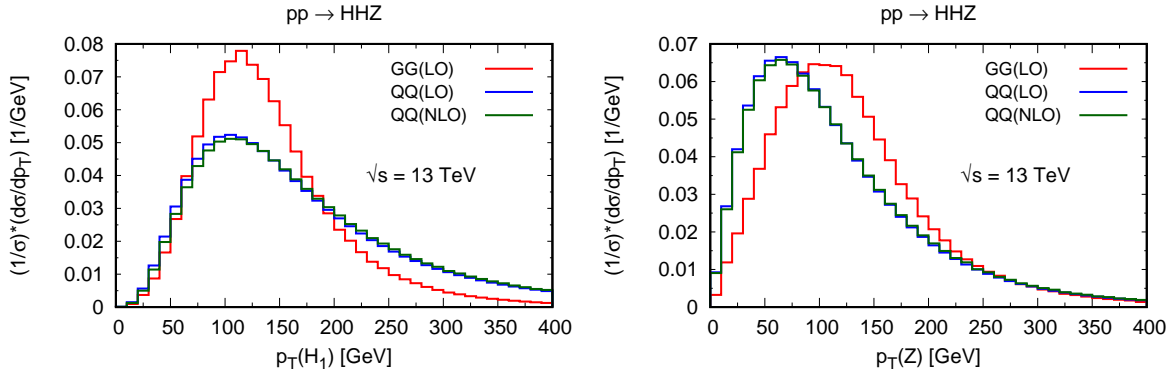


Figure 9: A comparison of normalized distributions for $p_T(H_1)$ and $p_T(Z)$ due to $gg \rightarrow HHZ$ and $qq \rightarrow HHZ$ in the SM at 13 TeV.

boson which has p_T distribution around 50 GeV with a significant tail. However, all three particles are produced mainly centrally. The leading Higgs bosons and Z boson are produced more back-to-back than the two Higgs bosons which are produced relatively closer to each other. These features are also reflected in di-boson invariant mass distributions. For example, M_{H_1Z} has harder tail than $M_{H_1H_2}$ and M_{H_2Z} . The partonic centre-of-mass energy around 500 GeV contributes most to the cross section. At higher center-of-mass energy, 100 TeV, the behavior of these distributions are similar. We further

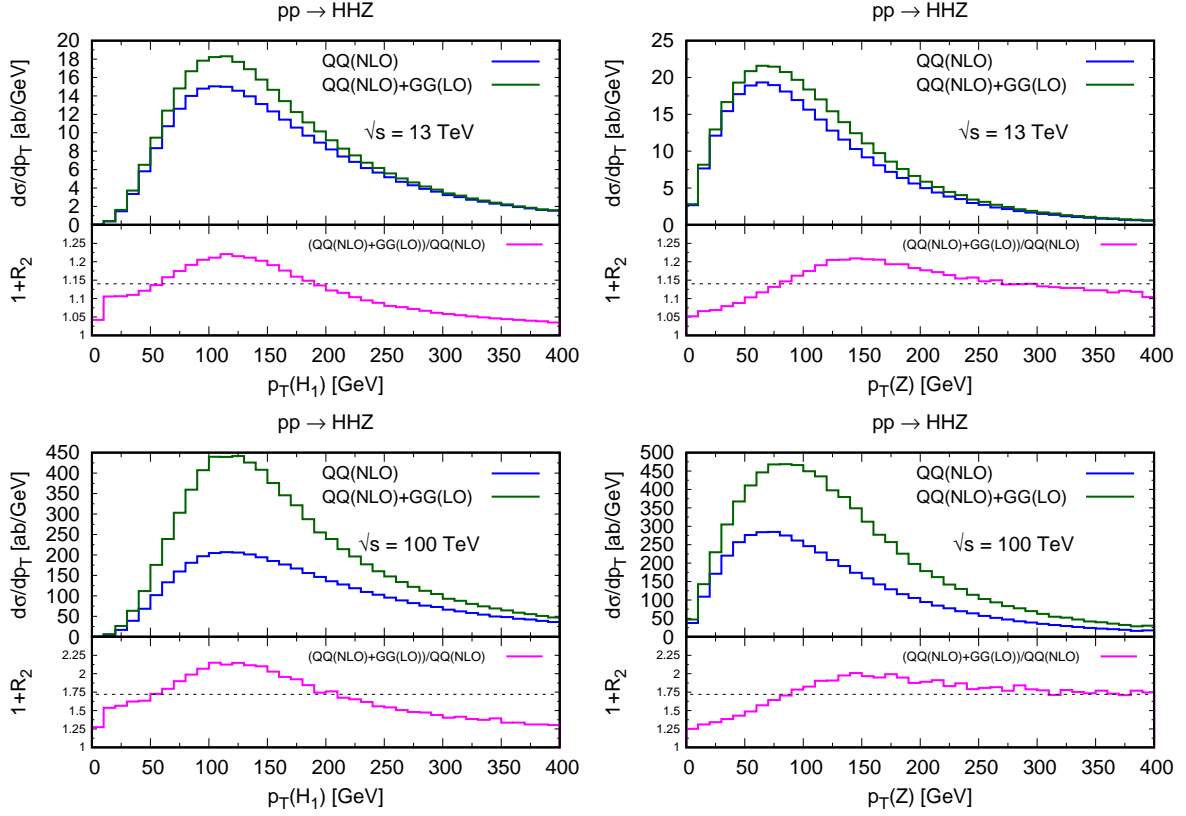


Figure 10: Combined $gg \rightarrow HHZ(\text{LO}) + qq \rightarrow HHZ(\text{NLO})$ contribution to $p_T(H_1)$ and $p_T(Z)$ distributions in the SM at 13 TeV and 100 TeV. Lower panels show the ratio of $QQ(\text{NLO}) + GG(\text{LO})$ and $QQ(\text{NLO})$ for each of these distributions. The dashed straight line in the lower panel of each plot refers to the same quantity at inclusive or total cross section level (see R_2 in Table 3).

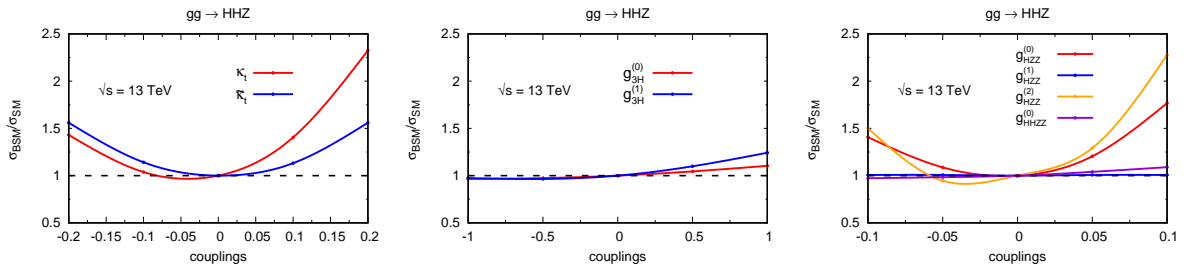


Figure 11: $\frac{\sigma_{\text{BSM}}}{\sigma_{\text{SM}}}$ as a function of anomalous couplings of the Higgs boson in $gg \rightarrow HHZ$ at 13 TeV.

compare the $GG(\text{LO})$ and $QQ(\text{LO and NLO})$ contributions in kinematic distributions for $p_T(H_1)$ and $p_T(Z)$ at 13 TeV LHC. In Fig. 9 we see that contribution of GG channel is characteristically different from that of QQ channel. The GG channel gives rise to softer events in $p_T(H_1)$, while harder events in $p_T(Z)$. These features remain true at higher centre-of-mass energies. In Fig. 10, we give the $p_T(H_1)$ and $p_T(Z)$ distributions combining $QQ(\text{NLO})$ and $GG(\text{LO})$ channels at 13 and 100 TeV. At the level of total cross section, the GG contribution is about 14% with respect to the $QQ(\text{NLO})$ contribution at 13 TeV. However, in the distributions the GG contribution can reach more than 20 % in certain bins. Similarly, at 100 TeV collider, although the contribution of the GG process to the total cross section is about 72% of the $QQ(\text{NLO})$ contribution (see Table 3), in the case of $p_T(H_1)$ between 100 – 200 GeV,

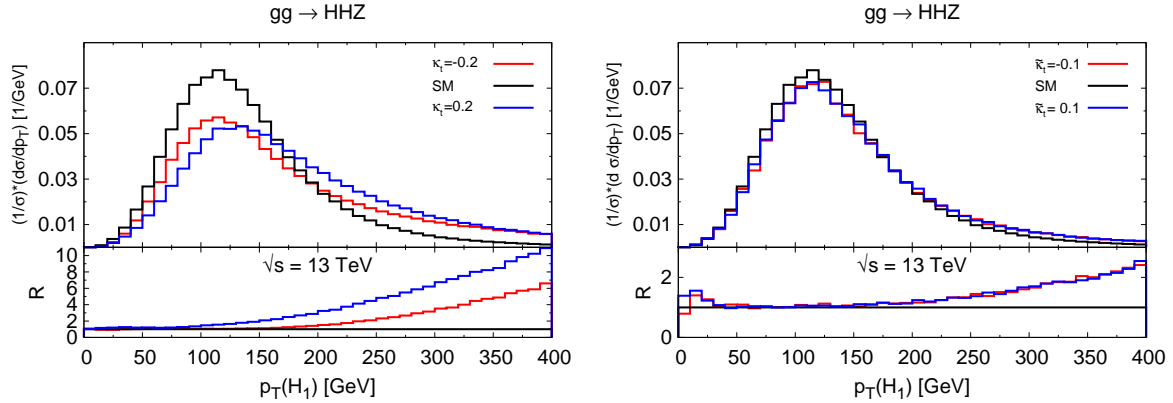


Figure 12: Normalized leading $p_T(H)$ distribution in $gg \rightarrow HHZ$ at 13 TeV for some benchmark values of anomalous top Yukawa couplings.

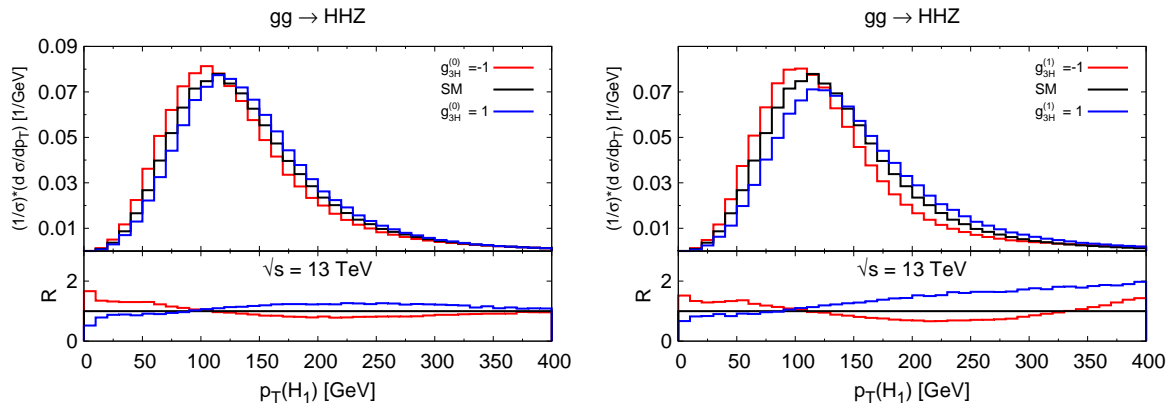


Figure 13: Normalized leading $p_T(H)$ distribution in $gg \rightarrow HHZ$ at 13 TeV for some benchmark values of HHH anomalous couplings.

the enhancement due to GG channel could be more than 100%.

The process $gg \rightarrow HHZ$ has four different couplings – ttH , HZZ , HHH , and $HHZZ$. In Fig. 11, we probe sensitivity of the production cross section to these anomalous couplings. The cross section is mainly sensitive to ttH and HZZ couplings. The scalar Yukawa coupling, κ_t , and the scaling coupling, $g_{HZZ}^{(0)}$, lead to largest modification. The cross section could double with allowed parameter range of these parameters. The effects of other anomalous couplings are rather modest. Like triple Higgs boson production, here also the $gg \rightarrow HHZ$ is not sensitive to $\tilde{\kappa}_t$ in the allowed parameter range mentioned in section 3. We find that tri-linear Higgs boson anomalous self-couplings do not play any significant role in this NNLO process. The derivative HZZ couplings and $HHZZ$ coupling also don't play any significant role in the allowed range mentioned in section 3. In Figs. 12, 13, 14, the effects of various anomalous couplings relevant to $gg \rightarrow HHZ$ on leading $p_T(H)$ distribution are shown. For that we take some benchmark values. We find that both κ_t and $\tilde{\kappa}_t$ lead to harder tail compared to the SM prediction. The contribution to the cross section at higher p_T is significantly large for higher κ_t . This may be a better avenue to see the effect of such interactions. Similar features are found for parameters $g_{HZZ}^{(0)}$ and $g_{HZZ}^{(2)}$. The effect of $g_{HZZ}^{(1)}$ is almost flat and remains close to SM prediction in all the bins. The dependence of the p_T distribution on $g_{HHZZ}^{(0)}$ is rather interesting. Compared to the SM values, this distribution is harder for the positive values of the anomalous coupling, and softer for the negative

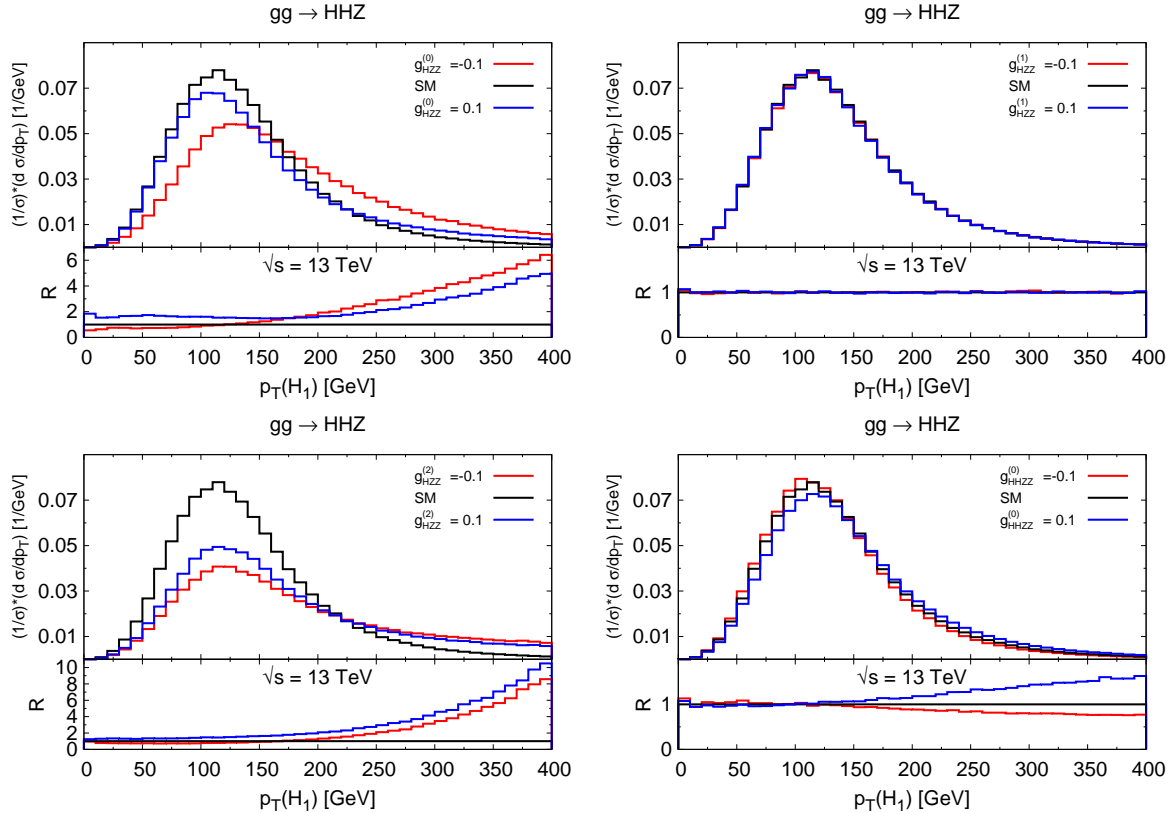


Figure 14: Normalized leading $p_T(H)$ distribution in $gg \rightarrow HHZ$ at 13 TeV for some benchmark values of HZZ and $HHZZ$ anomalous couplings.

values. There seems to be harder tail of this p_T distribution for larger values of $g_{3H}^{(1)}$, specially for the positive values. The distribution for $g_{3H}^{(0)}$ doesn't seem to show any special feature. The sensitivity of the NNLO process to anomalous interactions is similar at 100 TeV.

In this paper our focus has been the NNLO $gg \rightarrow HHZ$ process. That is why we have presented detailed results for this process. One may ask how sensitive is LO process to anomalous interactions. We have explored this sensitivity by using `Madgraph`. By including anomalous vertices, we find that LO quark-antiquark annihilation process is quite sensitive to anomalous derivative HZZ interaction. The cross section can increase by an order of magnitude. The increase is more at higher center-of-mass energy. This is unlike NNLO $gg \rightarrow HHZ$ process.

The process $pp \rightarrow HHZ$ is likely to be observable at the LHC. Including the NLO and NNLO corrections, the cross section is about 320 ab at 13 TeV. With the full integrated luminosity, one may expect around 1000 events. This process should be visible using various multilepton + jets signature. The main irreducible background of ZZZ has the cross section of 9.2 fb. But $Z \rightarrow b\bar{b}, \tau\tau$ branching ratios are smaller by a factor of 2-3 as compared to the Higgs boson decay. Then by restricting the number of jets in the signature, one may be able to detect this process. To look for evidence beyond the standard model, one may look for enhancement in large $p_T(Z)$ events. Reducible backgrounds, as mentioned above, may be tamed by flavor-tagging of jets. At higher energy machines, this process would definitely be observable.

6 Conclusions

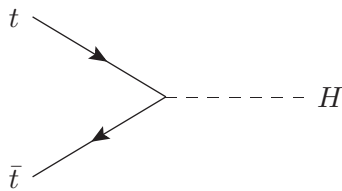
In this paper, we have considered the processes – $pp \rightarrow HHH, HH\gamma$, and HHZ . Our focus was on the gluon-gluon fusion contribution to them. The one-loop amplitude for the process $gg \rightarrow HH\gamma$ vanishes exactly. The process $pp \rightarrow HHH$ is important as it involves both trilinear and quartic Higgs boson couplings. A measurement of this process along with di-Higgs production can help in determining the form of the Higgs potential. It may be seen only if there exists anomalous interactions. This process is specially sensitive to trilinear Higgs boson couplings. This process can be observed at large center-of-mass energy machines with high luminosity. It will be challenging. The process $pp \rightarrow HHZ$ may be observable at the LHC after accumulation of 3 ab^{-1} luminosity. The GG(LO) contribution to this process is actually a NNLO contribution in α_s , and due to a large gluon flux it is 14% of the QQ(NLO) contribution to $pp \rightarrow HHZ$ at 13 TeV LHC. In certain kinematic windows GG(LO) contribution can be more than 20%. At a 100 TeV machine, $gg \rightarrow HHZ$ can be as important as $q\bar{q} \rightarrow HHZ$. This process is important, as it involves HHH and $HHZZ$ couplings and is background to triple Higgs production. The effect of $t\bar{t}H$ and HZZ anomalous couplings are more significant in the distributions than in the total cross section. This process can definitely be observed at higher energy, such as 100 TeV, machines with enough luminosity.

Acknowledgement

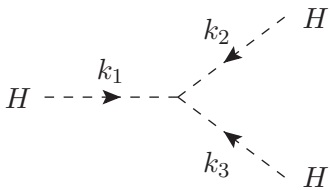
AS is supported by the MOVE-IN Louvain Cofund grant.

A Feynman Rules for anomalous Higgs vertices

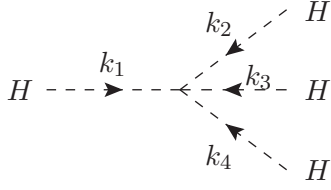
The Feynman rules for various anomalous couplings of the Higgs boson considered in section 3 are given below:



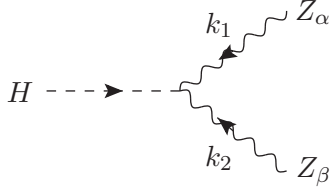
$$-i \frac{m_t}{v} \left\{ (1 + \kappa_t) + i \tilde{\kappa}_t \gamma_5 \right\}$$



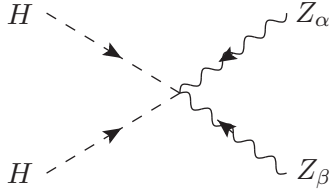
$$-i \frac{3m_H^2}{v} \left\{ (1 + g_{3H}^{(0)}) - \frac{g_{3H}^{(1)}}{3m_H^2} \sum_{j < k}^3 p_j \cdot p_k \right\}$$



$$-i \frac{3m_H^2}{v^2} \left\{ (1 + g_{4H}^{(0)}) - \frac{g_{4H}^{(1)}}{6m_H^2} \sum_{j < k}^4 p_j \cdot p_k \right\}$$



$$i \frac{gM_Z}{c_W} \left\{ g^{\alpha\beta} (1 + g_{HZZ}^{(0)}) + \frac{g_{HZZ}^{(1)}}{M_Z^2} [g^{\alpha\beta} (k_1 \cdot k_2) - k_2^\alpha k_1^\beta] + \frac{g_{HZZ}^{(2)}}{M_Z^2} [g^{\alpha\beta} (k_1^2 + k_2^2) - (k_1^\alpha k_1^\beta + k_2^\alpha k_2^\beta)] \right\}$$



$$i \frac{gM_Z}{c_W v} \left\{ g^{\alpha\beta} (1 + g_{HHZZ}^{(0)}) \right\}$$

References

- [1] ATLAS News, July 2017, URL <https://atlas.cern/updates/atlas-news/atlas-highlights-eps-hep-2017>
- [2] CMS News, July 2017, URL <https://cms.cern/news/cms-new-results-EPS-2017>
- [3] G. Aad *et al.* [ATLAS Collaboration], Phys. Lett. B **716**, 1 (2012)
- [4] S. Chatrchyan *et al.* [CMS Collaboration], Phys. Lett. B **716**, 30 (2012)
- [5] G. Aad *et al.* [ATLAS Collaboration], J. High Energy Phys. 12 (2015) 055.
- [6] G. Aaboud *et al.* [ATLAS Collaboration], J. High Energy Phys. 09 (2016) 001.
- [7] A. M. Sirunyan *et al.* [CMS Collaboration], Phys. Rev. Lett. 117 051802 (2016).
- [8] G. Aaboud *et al.* [ATLAS Collaboration], CERN-EP-2017-108, arXiv:1706.03731 [hep-ex].
- [9] A. M. Sirunyan *et al.* [CMS Collaboration], CERN-EP-2017-130, arXiv:1707.06193 [hep-ex].
- [10] G. Aaboud *et al.* [ATLAS Collaboration], CERN-EP-2017-082, arXiv:1706.04786 [hep-ex].
- [11] A. M. Sirunyan *et al.* [CMS Collaboration], CERN-EP-2017-097, arXiv:1706.03794 [hep-ex].

- [12] R. Aaij *et al.* [LHCb Collaboration], CERN-EP-2017-100, arXiv:1705.05802 [hep-ex].
- [13] P. Agrawal and G. Ladinsky, Phys. Rev. D **63**, 117504 (2001).
- [14] D. de Florian and Z. Kunszt, Phys. Lett. B **460**, 184 (1999).
- [15] S. Mao *et al.*, Phys. Rev. D **79**, 054016 (2009).
- [16] F. Campanario, J. High Energy Phys 10 (2011) 070.
- [17] T. Melia, K. Melnikov, R. Rontsch, M. Schulze and G. Zanderighi, J. High Energy Phys 08 (2012) 115.
- [18] P. Agrawal and A. Shivaji, Phys. Rev. D **86**, 073013 (2012).
- [19] P. Agrawal and A. Shivaji, J. High Energy Phys. 01 (2013) 071.
- [20] F. Campanario, Q. Li, M. Rauch and M. Spira, J. High Energy Phys. 06 (2013) 069.
- [21] A. K. Shivaji (*PhD Thesis*), arXiv:1305.4926 [hep-ph].
- [22] J. M. Campbell, R. K. Ellis, E. Furlan and R. Rontsch, Phys. Rev. D **90**, 093008 (2014).
- [23] P. Agrawal and Ambresh Shivaji, Phys. Lett. B **741**, 111 (2015).
- [24] B. Hespel, F. Maltoni and E. Vryonidou, JHEP **1506**, 065 (2015)
- [25] V. Hirschi and O. Mattelaer, J. High Energy Phys. 10 (2015) 146.
- [26] E. Gabrielli, B. Mele, F. Piccinini and R. Pittau, J. High Energy Phys. 07 (2016) 003.
- [27] F. Caola, K. Melnikov, R. Rontsch and L. Tancredi, Phys. Lett. B **754**, 275 (2016)
- [28] F. Caola, K. Melnikov, R. Rontsch and L. Tancredi, Phys. Rev. D **92**, no. 9, 094028 (2015)
- [29] J. M. Campbell, R. K. Ellis, Y. Li and C. Williams, J. High Energy Phys. 07 (2016) 148.
- [30] F. Caola, M. Dowling, K. Melnikov, R. Rontsch and L. Tancredi, J. High Energy Phys. 07 (2016) 087.
- [31] F. Granata, J. M. Lindert, C. Oleari and S. Pozzorini, arXiv:1706.03522 [hep-ph].
- [32] A. Shivaji, P. Agrawal and D. Saha, EPJ Web Conf. **129**, 00005 (2016)
- [33] T. Plehn and M. Rauch, Phys. Rev. D **72**, 053008 (2005).
- [34] T. Binoth *et al.*, Phys. Rev. D **74**, 113008 (2006).
- [35] F. Maltoni, E. Vryonidou and M. Zaro, J. High Energy Phys. 11 (2014) 079.
- [36] A. Papaefstathiou and K. Sakurai, J. High Energy Phys. 02 (2016) 006.
- [37] B. Fuks, J. H. Kim and S. J. Lee, Phys. Lett. B **771**, 354 (2017)
- [38] W. Kilian, S. Sun, Q. S. Yan, X. Zhao and Z. Zhao, J. High Energy Phys. 06 (2017) 145.
- [39] R. Frederix, S. Frixione, V. Hirschi, F. Maltoni, O. Mattelaer, P. Torrielli, E. Vryonidou and M. Zaro, Phys. Lett. B **732**, 142 (2014)

- [40] J. Baglio, A. Djouadi, R. Grber, M. M. Mhleitner, J. Quevillon and M. Spira, JHEP **1304**, 151 (2013)
- [41] D. Binosi, J. Collins, C. Kaufhold and L. Theussl, Comput. Phys. Commun. **180**, 1709 (2009)
- [42] C. Patrignani et al. (Particle Data Group), Chin. Phys. C, 40, 100001 (2016).
- [43] A. M. Sirunyan *et al.* [CMS Collaboration], arXiv:1707.02909 [hep-ex].
- [44] K. Whisnant, B. -L. Young and X. Zhang, Phys. Rev. D **52**, 3115 (1995).
- [45] K. Nishiwaki, S. Niyogi and A. Shivaji, J. High Energy Phys. **04** (2014) 011.
- [46] John. Ellis, Veronica. Sanz, Tevong. You J. High Energy Phys. **07**, 036 (2014).
- [47] W. Buchmller and D. Wyler, Nucl. Phys. B 268 (1986) 621.
- [48] B. Grzadkowski *et al.*, J. High Energy Phys. 10 (2010) 085.
- [49] R. Contino *et al.*, J. High Energy Phys. 07 (2013) 035.
- [50] J. A. Aguilar-Saavedra, Nucl. Phys. B **821**, 215 (2009).
- [51] V. Barger, T. Han, P. Langacker, B. McElrath and P. Zerwas, Phys. Rev. D **67**, 115001 (2003).
- [52] M.C. Gonzalez-Garcia Int. J. Mod. Phys. **A14** (1999) 3121.
- [53] K. Hagiwara, S. Ishihara, R. Szalapski and D. Zeppenfeld, Phys. Rev. D **48**, 2182 (1993).
- [54] B. Zhang, Y. -P. Kuang, H. -J. He and C. P. Yuan, Phys. Rev. D **67**, 114024 (2003).
- [55] J. A. M. Vermaseren, arXiv:math-ph/0010025.
- [56] S. Larin, Phys. Lett. B 303 113 (1992).
- [57] A. Shivaji, V. Ravindran and P. Agrawal, JHEP **1202**, 057 (2012)
- [58] G. J. van Oldenborgh and J. A. M. Vermaseren, Z. Phys. C **46**, 425 (1990).
- [59] A. van Hameren, Comput. Phys. Commun. **182**, 2427 (2011).
- [60] W. L. van Neerven and J. A. M. Vermaseren, Phys. Lett. B **137**, 241 (1984).
- [61] G.P. Lepage, VEGAS: An Adaptive Multi-dimensional Integration Program, Cornell preprint CLNS 80-447, March 1980.
- [62] S. Veseli, Comput. Phys. Commun. **108**, 9 (1998).
- [63] A. Geist et al., PVM: Parallel Virtual Machine (MIT Press, Cambridge, MA, 1994).
- [64] T. Appelquist and J. Carazzone, Phys. Rev. D **11**, 2856 (1975).
- [65] P. M. Nadolsky, H. L. Lai, Q. H. Cao, J. Huston, J. Pumplin, D. Stump, W. K. Tung and C.-P. Yuan, Phys. Rev. D **78**, 013004 (2008)
- [66] J. Alwall *et al.*, JHEP **1407**, 079 (2014)